Quench dynamics of thermal Bose gases across wide and narrow Feshbach resonances

Xiaoyi Yang and Ren Zhang[*]

MOE Key Laboratory for Nonequilibrium Synthesis and Modulation of Condensed Matter, Shaanxi Province Key Laboratory of Quantum Information and Quantum Optoelectronic Devices, School of Physics, Xi'an Jiaotong University, Xi'an 710049, China

Using high-temperature virial expansion, we study the quench dynamics of the thermal Bose gases near wide, narrow, and intermediate Feshbach resonances. Our results show that the shallow bound state near Feshbach resonances leads to oscillation of $\hat{n}_\mathbf{k}$. Near the wide Feshbach resonance, the long-time momentum distribution $\hat{n}_\mathbf{k}$ oscillates when the scattering length a_s is quenched to large but with finite positive values. The oscillation frequency is determined by the bound-state energy. When a_s is quenched to infinity or negative value, the oscillation vanishes. Near the narrow Feshbach resonance, when the background scattering length a_bg is larger than de Broglie wave length λ, there is an oscillation, and the frequency is determined by the energy of the shallow bound state in the open channel. When $a_\text{bg} < 0$ or $0 < a_\text{bg} \ll \lambda$, there is no shallow bound state in the open channel, and hence no oscillation. We check our conclusion using some realistic systems, and the results are consistent with our conclusion.

I. INTRODUCTION

Thanks to Feshbach resonances, the pairwise interaction between atoms can be controlled flexibly by tuning external fields, and the equilibrium properties in strongly interacting atomic gases have been extensively studied [1,2]. The timescale of the Hamiltonian manipulation can be much smaller than the relaxation time. As such, ultracold atomic gases have also become one of the most ideal platforms to investigate nonequilibrium physics, including the quench dynamics [3–9].

Here, quench dynamics refers to the evolution of initial states under an abruptly changed Hamiltonian. For instance, the s-wave scattering length a_s can be controlled by the magnetic field. When a_s is sinusoidally modulated by time-dependent external fields, the particle number of the noncondensation modes will exponentially grow, i.e., Bose-Einstein condensation (BEC) is depleted. If the modulation phase is suddenly changed by π, it was found that the excited particle number decreases, i.e., BEC revives [10]. Motivated by this phenomenon, a new kind of echo theory has also been proposed in BEC, which can be realized by quenching a_s or the trapping potential [11,12]. In the same spirit, there are many other studies on quench dynamics via quenching parameters of the Hamiltonian. Many-body localization and thermalization can be distinguished by the quench dynamics of the entanglement entropy [13]. The topology of Hamiltonian of band insulators can be extracted in the quench dynamics of the linking number [14–16]. The dynamical fractal has been established in quantum gases with discrete scaling symmetry [17].

In the seminal experiment by the Cambridge group [7], a series of universal quench dynamics of Bose gas have been revealed by quenching the interaction from zero to unitary. Both degenerate and thermal Bose gases of ^{39}K are studied near a Feshbach resonance located at $\sim$402.7G. This is a resonance of intermediate width, $s_\text{res} \sim 2.1$ [1]. In the follow-up theoretical studies, it has been treated as a wide one, and the comparison of theoretical and experimental results are satisfactory for both degenerate and thermal gases [18,19]. A natural question arises: What are the effects induced by resonance width? For ultracold Bose gases, the influence of few-body effects and short-range correlations has been extensively examined near a narrow Feshbach resonance, utilizing the two-channel zero-range model [20–22]. In this manuscript our attention is directed towards the dynamics of thermal Bose gases near both narrow- and intermediate-width Feshbach resonances. Our calculations employ a combination of the two-channel zero-range and square well models to describe the Feshbach resonance, while the dynamics of the momentum distribution is studied through the application of a virial expansion.

The virial expansion builds a connection between the few-body and the many-body physics [23–36]. It works well when comparing with experiments [37–44]. The control parameter is the fugacity $z = e^{\mu/(k_B T)}$, where μ is the chemical potential and k_B is the Boltzmann constant. At high temperature, μ is large and negative; therefore $z < 1$. Near both wide and narrow Feshbach resonances, this method has been applied to quantum gas in equilibrium [27,30,33,34,45–53]. Recently, it has also been implemented to the quench dynamics of Bose gas near a wide Feshbach resonance [19]. As such, it is natural to extend the virial expansion for dynamics to the narrow Feshbach resonance and a crossover from a wide one to a narrow one. Our main results are summarized in Table I.

This manuscript is organized as follows: In Sec. II, we introduce the virial expansion method and its application to quench dynamics. Section III focuses on the differences in quench dynamics near narrow and wide Feshbach resonances.

---

*renzhang@xjtu.edu.cn

TABLE I. Long-time behavior of the momentum distribution $n_\mathbf{k}$ dynamics near Feshbach resonance.

Resonance width	Oscillation	Nonoscillation
$s_{\text{res}} \gg 1$ (wide resonance)	s-wave scattering length, $a_s \gtrsim \lambda$	s-wave scattering $a_s < 0$ or $a_s = \infty$
$s_{\text{res}} \ll 1$ (narrow resonance) or $s_{\text{res}} \sim 1$ (intermediate width)	Background scattering length, $a_{\text{bg}} \gtrsim \lambda$	Background scattering length, $a_{\text{bg}} < 0$ or $0 < a_{\text{bg}} \ll \lambda$

We emphasize these differences using the two-channel square well model. In Sec. IV we investigate quench dynamics under different scenarios using the zero-range model. We consider variations in the s-wave scattering length a_s and the background scattering length a_{bg}. In Sec. V we consider realistic systems with different resonance widths and background scattering lengths. We demonstrate the conclusions reached in the previous sections within the context of these systems. Finally, we summarize the main findings of the paper and provide concluding remarks in Sec. VI.

II. VIRIAL EXPANSION FOR DYNAMICS

Let us first review the basics of virial expansion for quench dynamics. We consider thermal Bose gases with temperature T, then quench the interaction from zero to finite or unitary. The Hamiltonian becomes $\hat{H} = \hat{H}_0 + \hat{V}$, with $\hat{V}$ denoting the interaction. For later time $t > 0$, the system evolves under the full Hamiltonian $\hat{H}$ and eventually achieves a new equilibrium state. Some universal physics can be revealed in the prethermal process. To this end we could measure an observable $\hat{W}$, the expectation value $\mathcal{W}(t)$ of which can be written as [19]

$$\mathcal{W}(t) = \frac{\text{Tr}[e^{-\beta(\hat{H}_0 - \mu\hat{N})} e^{i\hat{H}t} \hat{W} e^{-i\hat{H}t}]}{\text{Tr}[e^{-\beta(\hat{H}_0 - \mu\hat{N})}]}, \quad (1)$$

where $\beta = 1/k_B T$ denotes the inverse temperature, and $\hat{N}$ is the total particle number of Bose gases. Here and hereafter, we set $\hbar = k_B = 1$ for convenience. The exact evaluation of $\mathcal{W}(t)$ is formidable in a many-body system because $\hat{W}$ does not commute with the Hamiltonian.

At high temperature we expand the observable $\mathcal{W}(t)$, instead of the thermodynamic potential Ω, in terms of the fugacity z. To the order of z^2, $\mathcal{W}(t)$ is expressed as

$$\mathcal{W}(t) = X_1 z + (-Q_1 X_1 + X_2)z^2 + O(z^3). \quad (2)$$

Here, X_n and Q_n are defined as

$$X_n = \text{Tr}_n[\Theta(t)e^{-\beta\hat{H}_0} e^{i\hat{H}t} \hat{W} e^{-i\hat{H}t}]$$
$$= \sum_{\alpha,\gamma,\kappa} e^{-\beta E_\alpha^{(n)}} G_{\kappa\alpha}^{(n)}(t)\langle\psi_\kappa^{(n)}|\hat{W}|\psi_\gamma^{(n)}\rangle G_{\gamma\alpha}^{(n)}(t), \quad (3)$$

$$Q_n = \text{Tr}_n[e^{-\beta\hat{H}_0}], \quad (4)$$

respectively; $n = 1, 2 \ldots$ denotes the particle number; $E_\alpha^{(n)}$ and $\psi_\alpha^{(n)}$ represent the energy and wave function of the n-particle noninteraction state, respectively. $\Theta(t)$ is the step function. $G^{(n)}(t)$ is the retarded Green's function of the

n-particle interacting system and is defined as

$$G_{\gamma\alpha}^{(n)}(t) = \langle\psi_\gamma^{(n)}|\Theta(t)e^{-it\hat{H}}|\psi_\alpha^{(n)}\rangle$$
$$= \frac{i}{2\pi} \int_{-\infty}^{\infty} d\omega e^{-i\omega t} G_{\gamma\alpha}^{(n)}(\omega + i0^+). \quad (5)$$

Therefore, by solving the n-particle problem we can determine the evolution of the many-body system, with the accuracy improving as we increase n.

The same as the experiment, we consider the dynamics of the particle number in the $\mathbf{k}$ mode, i.e., $\hat{W} = \hat{n}_\mathbf{k}$. For a single particle system, $\hat{H} = \hat{H}_0$, and

$$X_1 = \text{Tr}_1[\Theta(t)e^{-\beta\hat{H}_0} e^{it\hat{H}_0} \hat{n}_\mathbf{k} e^{-it\hat{H}_0}] = e^{-\beta\mathbf{k}^2/(2m)}. \quad (6)$$

Therefore X_1 and Q_n are independent of time t. The evolution of momentum distribution $\delta n_\mathbf{k} = n_\mathbf{k}(t) - n_\mathbf{k}(0)$ depends only on X_2 in Eq. (2), i.e.,

$$\delta n_\mathbf{k} = [X_2(t) - X_2(0)]z^2, \quad (7)$$

which can be obtained by solving the two-body problem. For the two-body problem, the noninteracting wave function is labeled by $|\psi_a^{(2)}\rangle = |\mathbf{P}, \mathbf{q}\rangle$, with $\mathbf{P}$ and $\mathbf{q}$ being the total and relative momentum of two bosons, respectively. The corresponding energy reads $E_a^{(2)} = P^2/(4m) + q^2/m$, where m is the reduced mass. According to the Lippmann-Schwinger function, the retarded Green's function can be written as

$$G_{\alpha\beta}^{(2)}(s) = G_{0\alpha\beta}(s) + G_{0\alpha\beta}(s)T_2(s)G_{0\alpha\beta}(s)$$
$$= \left[\frac{\langle\mathbf{q}_\alpha|\mathbf{q}_\beta\rangle}{s - \varepsilon_{\mathbf{q}_\alpha}} + \frac{T_2(s)}{(s - \varepsilon_{\mathbf{q}_\alpha})(s - \varepsilon_{\mathbf{q}_\beta})}\right]\delta_{\mathbf{P}_\alpha,\mathbf{P}_\beta}, \quad (8)$$

where $s = \omega + i0^+$, $\varepsilon_{\mathbf{q}_\alpha} = \mathbf{q}_\alpha^2/m$ is the kinetic energy of the relative motion, and $T_2(s)$ denotes the T matrix of the two-body scattering. We have also used the free Green's function for the relative motion $G_0(s) = (s - \mathbf{q}^2/m)^{-1}$ in the second line of Eq. (8).

III. WIDE AND NARROW RESONANCES

Before embarking on the difference between wide and narrow resonance, let us recall the two-body scattering theory. The generic relation between scattering amplitude $f(\mathbf{k}' \leftarrow \mathbf{k})$ and scattering T matrix $T(\mathbf{k}', \mathbf{k}; E)$ is $f(\mathbf{k}' \leftarrow \mathbf{k}) = -\frac{m}{4\pi}T_2(\mathbf{k}', \mathbf{k}; E)$. For the partial-wave scattering, the scattering amplitude $f_\ell(k)$ is defined by the partial-wave scattering matrix $s_\ell = e^{2i\delta_\ell}$,

$$f_\ell(k) = \frac{s_\ell - 1}{2ik} = -\frac{1}{ik - k/\tan\delta_\ell(k)}, \quad (9)$$

where $\delta_\ell(k)$ is the energy-dependent phase shift of the ℓth partial wave. In this manuscript we consider the s-wave scattering, and the T matrix is written as

$$T_2(s) = \frac{4\pi/m}{-\sqrt{ms}/\tan\delta_0 - \sqrt{-ms}}. \quad (10)$$

In the effective-range theory, $\sqrt{ms}/\tan\delta_0 = -1/a_s + r_{\text{eff}}ms/2 + \cdots$, with a_s and r_{eff} denoting the s-wave scattering length and the effective range, respectively. For wide resonance, the effective-range effect can be ignored,

and a_s is the only parameter to characterize the interaction. For narrow resonance, one has to include the effective range to incorporate the energy-dependence of the phase shift. For the van der Waals interaction, the quantum defect theory can give the exact phase shift [54,55]. For simplicity, we consider a two-channel square well model to mimic the interaction between atoms [1,2]. In the basis spanned by the closed and open channel, the interaction can be written as

$$
\hat{V}(r) = \begin{cases} \begin{bmatrix} -V_o & W \\ W & -V_c + \delta\mu_B B \end{bmatrix}, & \text{for } r < r_0; \\ \begin{bmatrix} 0 & 0 \\ 0 & \infty \end{bmatrix}, & \text{for } r > r_0, \end{cases}
\tag{11}
$$

where V_c and V_o represent the closed-channel and open-channel potential, and W is the inter-channel coupling strength. r_0 is the potential range, and the corresponding energy scale is $E_0 = 1/(mr_0^2)$. $\delta\mu_B$ is the magnetic momentum difference between the closed and open channel. By tuning the magnetic field, a series of Feshbach resonances appear (refer to Appendix A). Although this toy model does not quantitatively capture the interaction potential detail, it provides a reliable qualitative picture. By solving the two-channel model, the effective phase shift can be analytically obtained. Upon substituting the phase shift into Eqs. (10) and (8), the evolution of momentum distribution $\delta n_\mathbf{k}(t)$ can be obtained. To precisely distinguish wide and narrow Feshbach resonance, we define the parameter

$$
s_{\text{res}} = \frac{a_{\text{bg}}}{r_0} \frac{\delta\mu_B \Delta}{E_0},
\tag{12}
$$

where a_{bg} is the background scattering length determined by V_o. Δ is the magnetic field width of the resonance. $s_{\text{res}} \gg (\ll)1$ indicates a wide (narrow) resonance; when $s_{\text{res}} \sim 1$, it is of intermediate width.

In Fig. 1 we depict $\sin^2\delta_0$ as a function of the magnetic field and incident energy for both wide resonance (a) and narrow resonance (b). The $s_{\text{res}} \sim 260$ and $s_{\text{res}} \sim 0.04$ for the wide and narrow resonance. When $\delta_0 = \pi/2$, i.e., $\sin^2\delta_0 = 1$, the resonance happens. It is clear that the phase shift of wide resonance almost does not depend on the incident energy, as shown in (a). In contrast, the phase shift of narrow resonance strongly depends on the incident energy, as shown in (b). For both cases we quench the interaction by abruptly changing the magnetic field to B_{res}, the position of resonance, and measure the dynamics of momentum distribution. Near the wide resonance, the low-momentum ($k\lambda < 4.5$) $\delta n_\mathbf{k}$ decreases monotonically after quenching and tends to a stable value after a long-time evolution; the high-momentum ($k\lambda > 4.5$) $\delta n_\mathbf{k}$ increases monotonically and tends to a stable value after a long-time evolution. There is a critical momentum ($k\lambda = 4.5$), where $n_\mathbf{k}$ goes up and down, and tends to its initial value. This observation is consistent with experimental results [7] and theoretical results given by the zero-range potential [19]. Here $\lambda = \sqrt{2\pi/(mT)}$ denotes the thermal de Broglie wavelength, and we define a time unit $t_\lambda = 1/T$. However, near the narrow resonance, the momentum distribution dynamics show very different behavior in contrast to their wide resonance counterpart. Although the tendency of $\delta n_\mathbf{k}$ for low and high momentum remains, there is oscillation with damping amplitude, which means that there must be an intrinsic energy
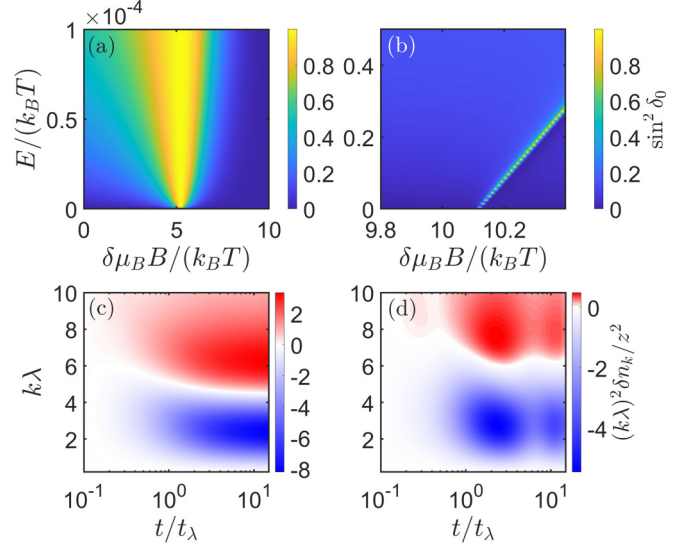

FIG. 1. The phase shift $\sin^2\delta_0$ and momentum distribution $\delta n_\mathbf{k}$ evolution of thermal Bose gas near wide and narrow resonance. The interaction is quenched by abruptly changing the magnetic field to resonance. $s_{\text{res}} = 260$ for the wide resonance (a), $s_{\text{res}} = 0.003$ and $a_{\text{bg}} = 0.3\lambda$ for the narrow resonance (b). (c) Near the wide resonance, the low-momentum $n_\mathbf{k}$ monotonically decreases and the high-momentum $n_\mathbf{k}$ monotonically increases. The critical momentum is around $k\lambda = 4.5$. (d) Near the narrow resonance, $n_\mathbf{k}$ shows damped oscillation when it decreases or increases.

scale near the narrow resonance. The critical momentum shifts slightly.

IV. ZERO-RANGE MODEL

To gain insight into this phenomenon, let us examine the zero-range model. For the wide resonance, the two-channel model in Eq. (11) can be approximated by a zero-range single-channel model. The two-body scattering T matrix $T_2(s)$ reduces to

$$
T_2(s) = \frac{4\pi/m}{a_s^{-1} - \sqrt{-ms}}.
\tag{13}
$$

The pole of $T_2(s)$ gives the energy of the shallow bound state, $E_b = -1/(ma_s^2)$. When the interaction is quenched to unitary, i.e., $a_s = \infty$, the bound-state energy vanishes. The Hamiltonian is scale invariant, and the only relevant length scales are the interparticle spacing and the thermal de Broglie wavelength. As such, the dynamics driven by the scale-invariant Hamiltonian are universal. Nevertheless, when a_s is quenched to a positive finite value, this extra length scale would exhibit itself in the dynamics.

In Fig. 2 we show the momentum distribution dynamics when the quenched interaction deviates from the resonance position. For final $a_s > 0$, we observe a long-time oscillation in the momentum distribution dynamics, as shown in (a), similar to that near the narrow resonance. The oscillation frequency for different momentum is the same, as depicted in (c). We extract the oscillation frequency for varying a_s. To this end we apply the fast Fourier transform to the oscillation part of $\delta n_\mathbf{k}$. This allows us to obtain a spectrum $\mathcal{A}(\omega)$, which
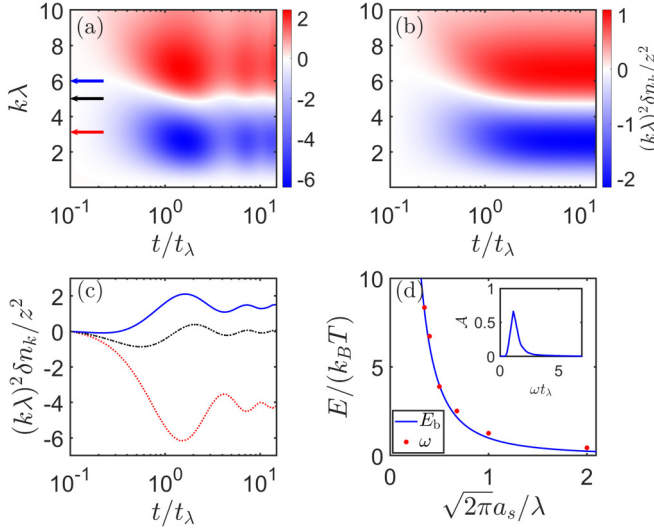
FIG. 2. The evolution of the momentum distribution when the quenched interaction deviates from the resonance position. (a) Final $a_s = \lambda/\sqrt{2\pi}$. (b) Final $a_s = -\lambda/\sqrt{2\pi}$. (c) $\delta n_{\mathbf{k}}$ evolution for three particular momentums: blue solid line ($k\lambda = 6$), black dashed-dotted (cross momentum), red dashed line ($k\lambda = 3$). (d) The shallow bound-state energy $|E_b| = 1/(ma_s^2)$ and oscillation frequency ω of the momentum dynamics. The value of ω closely follows the bound-state energy. Inset: The spectrum $\mathcal{A}(\omega)$ for the final $a_s = \lambda/\sqrt{2\pi}$.

represents the distribution of frequencies present in the oscillations. By analyzing the location of the peak in this spectrum, we can identify the dominant frequency associated with the oscillations. Our results show that the value of frequency ω closely follows the bound-state energy $|E_b| = 1/(ma_s^2)$, as shown in (d). Therefore we conclude that the oscillation in dynamics originates from the shallow bound state. When the final $a_s < 0$, there is no shallow bound state and hence no oscillation in the dynamics, as shown in (b).

Now we turn to the dynamics near the narrow- or intermediate-width Feshbach resonance, where the single-channel model is not sufficient to characterize the interaction. As such, we need to adopt the two-channel zero-range model [56], the two-body scattering T matrix T_2 of which can be written as (refer to Appendix B)

$$T_2(s) = \frac{4\pi/m}{\frac{s - \delta\mu_B(B - B_{\text{res}})}{a_{\text{bg}}[s + \delta\mu_B\Delta - \delta\mu_B(B - B_{\text{res}})]} - \sqrt{-ms}}, \quad (14)$$

where B_{res} denotes the magnetic field at resonance. The pole of $T_2(s)$ in Eq. (14) gives two bound states. By substituting Eq. (14) into Eq. (8), we can evaluate the momentum distribution $n_{\mathbf{k}}$.

Figure 3(a) shows the momentum distribution dynamics of $n_{\mathbf{k}}$ after quenching the interaction to resonance. We compare the results of the two-channel square model (solid curves) and zero-range model (dashed curves) for some particular momentum. Near the narrow resonance ($s_{\text{res}} = 0.003$), both results show that there is a long-time oscillation, but the frequencies are different. Near resonance of intermediate width ($s_{\text{res}} = 2$), the dynamics are almost the same as that near the wide resonance. This explains why the single-channel model gives consistent results with the experiment. Another
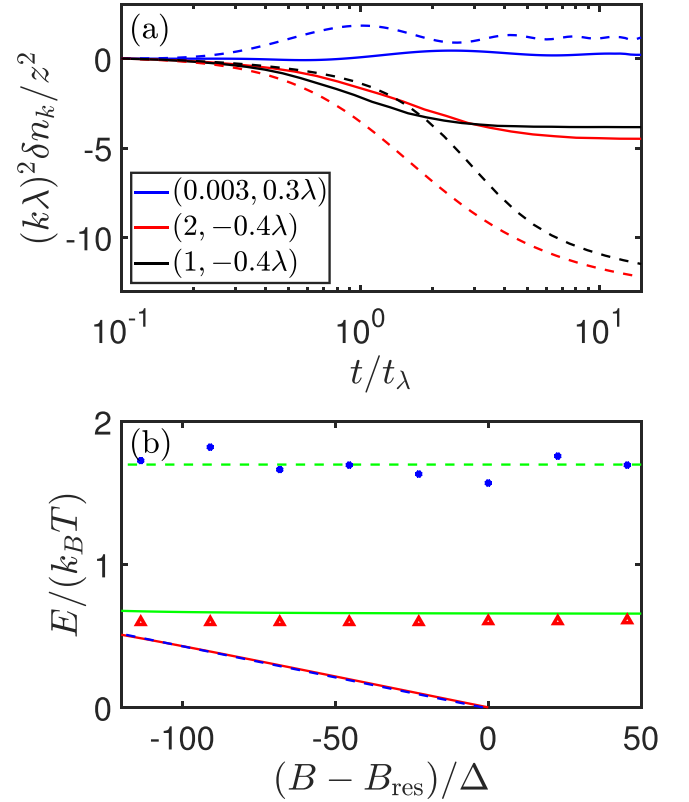

FIG. 3. The evolution of the momentum distribution after quenching the interaction to resonance. (a) Dynamics of $n_{\mathbf{k}}$ near the narrow and intermediate Feshbach resonance. The numbers in the legend represent ($s_{\text{res}}, a_{\text{bg}}$). Solid (dashed) curves represent two-channel square (zero-range) model. $k\lambda = 7(3)$ for narrow (intermediate) resonance. (b) Binding energy given a two-channel square (solid lines) and zero-range (dashed lines) model. The green lines indicate the bound-state energy in the open channel. The blue circle and red triangle are the oscillation frequency extracted from the dynamics of $n_{\mathbf{k}}$.

important observation is that when $a_{\text{bg}} < 0$, $\delta n_{\mathbf{k}}$ also exhibits a monotonically decreasing behavior near the intermediate resonance ($s_{\text{res}} = 1$), as indicated by the black curves. This behavior arises due to the absence of a shallow bound state in the open channel.

Near the narrow resonance, the oscillation frequency ω is determined by the binding energy of the open-channel bound state instead of the shallow bound state near the threshold. In Fig. 3(b) we present the binding energy given by the two-channel square model and zero-range model. The binding energies at the threshold of these two models are the same, as illustrated by the blue dashed and red solid lines. However, the other bound states originate from the open channel, and binding energies given by these two models are different, as shown by the green dashed and green solid lines. We extract the oscillation frequency near narrow resonance in Fig. 3(a). It closely follows the binding energy of the bound state in the open channel, instead of that at the threshold. The importance of the open-channel bound state near a narrow resonance can be understood as follows: In the long-range regime, there is no coupling between the open and closed channels, and the
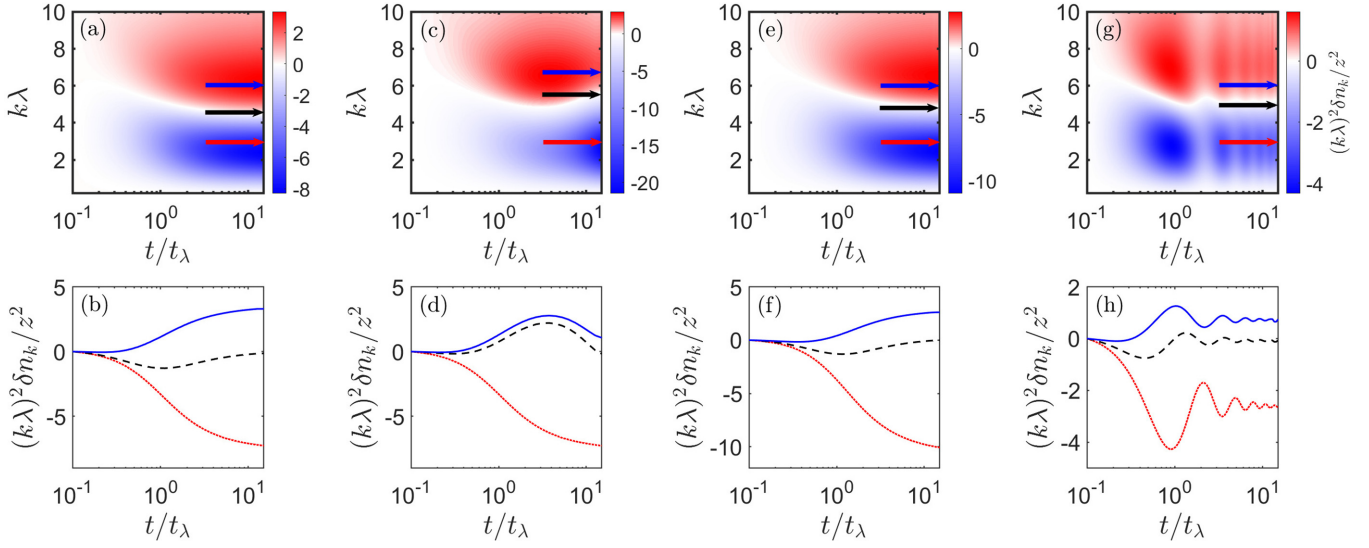
FIG. 4. The dynamics of $\delta n_{\mathbf{k}}$ for realistic systems near Feshbach resonance. (a, b) ^{133}Cs near the wide resonance with $s_{\text{res}} = 560$. (c, d)^{133}Cs near the intermediate resonance with $s_{\text{res}} = 0.67$ and $a_{\text{bg}} = 926a_0$. (e, f) ^{7}Li near the intermediate resonance with $s_{\text{res}} = 0.8$ and $a_{\text{bg}} = -25a_0$. (g, h) ^{133}Cs near the narrow resonance with $s_{\text{res}} = 0.002$ and $a_{\text{bg}} = 160a_0$. Here a_0 is Bohr's radius.

atoms primarily occupy the open channel. However, as they come closer in the short-range regime, the coupling between these channels becomes significant, resulting in the atoms existing in superposition states involving both the open and closed channels. However, near a narrow resonance, the coupling strength W between the two channels is relatively weak. As a result, the bound state in the open channel becomes dominant and governs the oscillation behavior observed in the dynamics.

V. APPLICATION TO REALISTIC SYSTEMS

We show the quench dynamics of some realistic systems. Here we consider four different systems including wide, narrow, and intermediate resonance [1]. (I) We choose ^{133}Cs near a wide resonance with $s_{\text{res}} = 560$. When the interaction is quenched to unitary, the evolution of the momentum distribution is the same as that near the wide resonance, as shown in Fig. 4(a). (II) In contrast, for ^{133}Cs near the narrow resonance with $s_{\text{res}} = 0.002$ and $a_{\text{bg}} = 160a_0$ (a_0 is the Bohr radius), shown in Fig. 4(d), we see that the momentum distribution oscillates, which originates from the bound state in the open channel. (III) For quench dynamics near resonance of intermediate width, we choose two systems, ^{133}Cs near resonance with $s_{\text{res}} = 0.67$ (b) and ^{7}Li near resonance with $s_{\text{res}} = 0.8$ (c). However, the background scattering lengths are different for these two systems. For ^{133}Cs, $a_{\text{bg}} = 926a_0$ implies a shallow bound state in the open channel, and we see that the momentum distribution oscillates. Nevertheless, for ^{7}Li, $a_{\text{bg}} = -25a_0$, there is no shallow bound state in the open channel and thus no oscillation in the momentum distribution.

VI. CONCLUSION

In summary, we used virial expansion to study quench dynamics across the wide and narrow Feshbach resonances. Taking the dynamics of momentum distribution as an

example, we showed the dynamics can be affected by the bound state, and the frequency of oscillation is determined by the energy of the bound state. Specifically, near the wide resonance, the relevant bound state is the shallow bound state near the threshold, while near the narrow or intermediate-width resonance, the relevant bound state is the bound state of the open channel. We checked our conclusion using some realistic systems. A three-body bound state leads to interesting effects in ultracold Bose gas [57–59]. It is worth investigating the three-body effect in the dynamics of thermal Bose gas in future studies.

APPENDIX A: TWO-CHANNEL SQUARE WELL MODEL

We here solve the two-channel square model to show Feshbach resonances and use a spherical box potential V with the interaction range of r_0 to describe the interaction between two atoms. We consider the s-wave scattering, so that the radial wave function is given by $\Psi = \chi/r$, with Ψ being the wave function. χ satisfies the Schrödinger equation,

$$-\frac{1}{m}\frac{d^2\chi}{dr^2}\mathbb{I} + V(r)\chi = E\chi, \qquad (A1)$$

$$V(r) = \begin{cases} \begin{bmatrix} -V_o & W \\ W & -V_c + \delta\mu_B B \end{bmatrix}, & \text{for } r < r_0; \\[2mm] \begin{bmatrix} 0 & 0 \\ 0 & \infty \end{bmatrix}, & \text{for } r > r_0, \end{cases} \qquad (A2)$$

where m is the mass of particles, V_c and V_o represent the closed-channel $|c\rangle$ and open-channel $|o\rangle$ potential, and W is the interchannel coupling strength. $\delta\mu_B$ is the magnetic momentum difference between closed and open channel. $\mathbb{I}$ denotes the 2×2 identity.

At the distance $r > r_0$, the wave function is written as

$$\chi = A \sin(kr + \delta_0)|o\rangle, \tag{A3}$$

while at a distance $r < r_0$, those two channels are coupled. We define a set of bases $|+\rangle$ and $|-\rangle$ such that the wave function and the Hamiltonian are diagonalized. Thus the wave function can be rewritten as $\chi = \chi_+|+\rangle + \chi_-|-\rangle$, and the bases $|\pm\rangle$ are a superposition of $|o\rangle$ and $|c\rangle$:

$$\begin{bmatrix} |+\rangle \\ |-\rangle \end{bmatrix} = \begin{bmatrix} \cos\theta & \sin\theta \\ -\sin\theta & \cos\theta \end{bmatrix} \begin{bmatrix} |o\rangle \\ |c\rangle \end{bmatrix}. \tag{A4}$$

In the region $r < r_0$, the wave function satisfies the boundary condition $\chi(r = 0) = 0$, and the solution is given by

$$\chi_\pm = C \sin(\sqrt{m(E - V_\pm)}r), \tag{A5}$$

where

$$V_\pm = \frac{-V_c - V_o + \delta\mu_B B}{2} \pm \frac{1}{2}\sqrt{(V_c - V_o - \delta\mu_B B)^2 + 4W^2}. \tag{A6}$$

Considering the boundary condition at $r = r_0$, the closed-channel wave function vanishes and the open-channel wave function keeps the continuum. With the solution given in Eqs. (A3) and (A5), we obtain

$$\frac{k}{\tan\delta_0} = \sqrt{m(E - V_+)} \cot[\sqrt{m(E - V_+)}r_0] \cos^2\theta$$
$$+ \sqrt{m(E - V_-)} \cot[\sqrt{m(E - V_-)}r_0] \sin^2\theta. \tag{A7}$$

The relation between the scattering amplitude and the T matrix reads

$$f_0(k) = -\frac{1}{ik - k\cot\delta_0} = -\frac{m}{4\pi}T_2(\mathbf{k}', \mathbf{k}; E), \tag{A8}$$

and thus we obtain the two-body scattering T matrix with the phase shift given in Eq. (A7).

Next we consider the bound-state energy. At the distance $r > r_0$, the wave function of bound state is written as

$$\chi = e^{-k_b r}|o\rangle. \tag{A9}$$

At distance $r < r_0$, the same as Eq. (A5), the solution is given by

$$\chi_\pm = D \sin\left[\sqrt{m(-k_b^2 - V_\pm)}r\right]. \tag{A10}$$

By matching the boundary condition at $r = r_0$, we obtain

$$-k_b = \sqrt{m(-k_b^2 - V_+)} \cot\left[\sqrt{m(-k_b^2 - V_+)}r_0\right] \cos^2\theta$$
$$+ \sqrt{m(-k_b^2 - V_-)} \cot\left[\sqrt{m(-k_b^2 - V_-)}r_0\right] \sin^2\theta. \tag{A11}$$

The solution k_b of Eq. (A11) should be a positive real.

In order to distinguish wide and narrow resonances, we can define the parameter s_{res} as

$$s_{\text{res}} = \frac{a_{\text{bg}}}{r_0}\frac{\delta\mu_B\Delta}{E_0}, \tag{A12}$$

where a_{bg} is the background scattering length, Δ is the resonance width, and $E_0 = 1/(mr_0^2)$. The background scattering length a_{bg} is determined by the open channel:

$$a_{\text{bg}} = \sqrt{-mV_o} \cot(\sqrt{-mV_o}r_0). \tag{A13}$$

Figure 5(a) shows the scattering length a_s of resonances with $s_{\text{res}} = 260$, and it diverges at the position of resonance $\delta\mu_B B_{\text{res}} = 5.2k_B T$. Figure 5(c) shows a broad region of phase shift near B_{res} where $\sin^2\delta_0 \approx 1$, and it remains stable when the incoming energy increases. Figure 5(d) shows the binding energy near the threshold, The solid line represents the binding energy given by Eq. (A11), which is consistent with the energy $E = -\hbar^2/(ma_s^2)$. In this resonance we can also find another bound-state energy, but its energy is four to five orders of magnitude smaller.

Figure 5(b) shows the scattering length of narrow resonances with $s_{\text{res}} = 0.04$. Figure 5(f) shows the binding energy near these resonances. First we can see the energy given by the exact solution no longer matches the energy given by the single-channel model. This means that when dealing with narrow resonance-related problems, we should use the two-channel model. Second, we obtain two bound states near the position of resonance, and one of the energies is near the threshold (solid line). The deeper energy is mainly contributed by the open channel, which is represented by the dashed line. Here we choose $V_o = 4.68k_B T$, and thus the bare bound-state energy supported by the open channel is $E_b = 0.75k_B T$, which is close to the deeper binding energy.

APPENDIX B: T MATRIX OF TWO-CHANNEL ZERO-RANGE MODEL

In this section we derive the T matrix of the two-channel zero-range model. With a contact potential, the second-quantized Hamiltonian in the momentum space can be written as

$$\hat{\mathcal{H}} = \sum_{\mathbf{k}} \frac{\mathbf{k}^2}{2m}\hat{\Psi}_{\mathbf{k}}^\dagger\hat{\Psi}_{\mathbf{k}} + \sum_{\mathbf{k}}\left(\frac{\mathbf{k}^2}{4m} + \nu\right)\hat{b}_{\mathbf{k}}^\dagger\hat{b}_{\mathbf{k}}$$
$$+ \frac{g}{V}\sum_{\mathbf{k},\mathbf{k}_1,\mathbf{k}_2}\Psi_{\frac{\mathbf{k}}{2}+\mathbf{k}_1}^\dagger\Psi_{\frac{\mathbf{k}}{2}-\mathbf{k}_1}^\dagger\Psi_{\frac{\mathbf{k}}{2}-\mathbf{k}_2}\Psi_{\frac{\mathbf{k}}{2}+\mathbf{k}_2}$$
$$+ \frac{\alpha}{\sqrt{V}}\sum_{\mathbf{k},\mathbf{k}_1}\Psi_{\frac{\mathbf{k}}{2}+\mathbf{k}_1}^\dagger\Psi_{\frac{\mathbf{k}}{2}-\mathbf{k}_1}^\dagger\hat{b}_{\mathbf{k}} + \hat{b}_{\mathbf{k}}^\dagger\Psi_{\frac{\mathbf{k}}{2}-\mathbf{k}_1}\Psi_{\frac{\mathbf{k}}{2}+\mathbf{k}_1}. \tag{B1}$$

Here g is the bare interaction between open-channel atoms themselves, $\Psi_\sigma^\dagger$ and Ψ_σ are the creation and annihilation
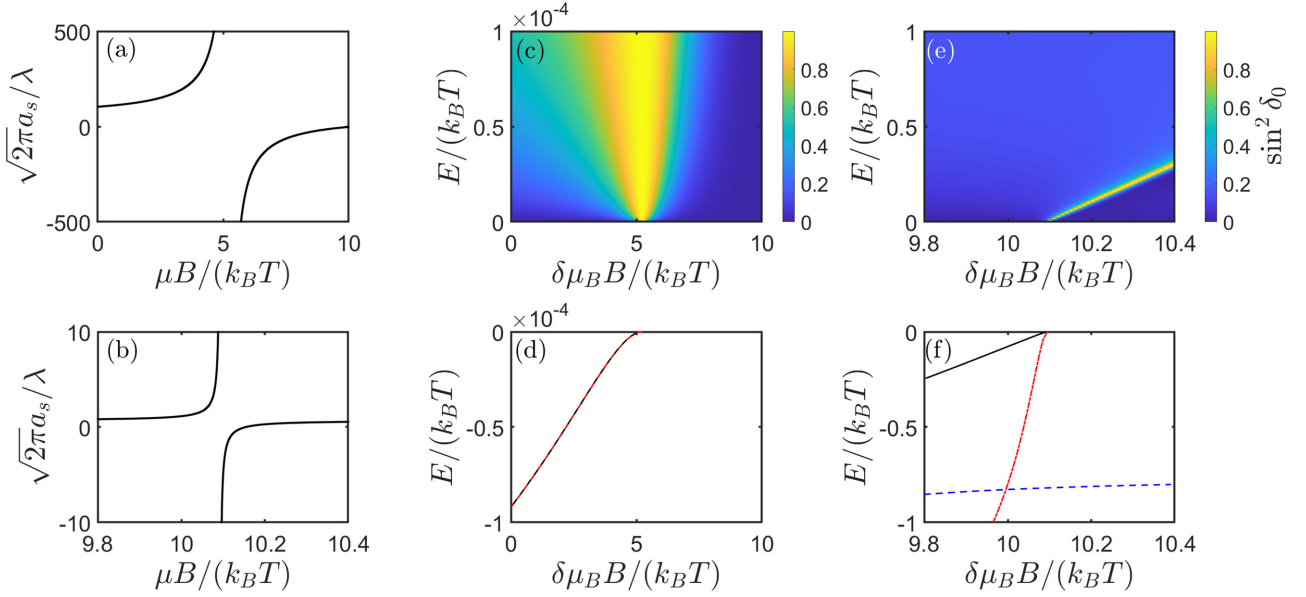
FIG. 5. Feshbach resonance scattering lengths and the binding energies. (a, b) The scattering length a_s changes with magnetic field strength B under the wide and narrow resonances, respectively. (c, e) Changes of $\sin^2 \delta_0$ with energy E. (d, f) Energy of the bound state where the solid line represents the binding energy given by Eq. (A11), the red dot-dashed line represents the binding energy given by $E = -\hbar^2/(m a_s^2)$, and the blue dashed line in (f) represents another binding energy under narrow resonances. Here we choose $V_c = 20 k_B T$, $V_o = 2.5 k_B T$, and the coupling strength $W = 0.5 k_B T$ as wide resonances in (a), (c), and (d), respectively, and $V_c = 20 k_B T$, $V_o = 4.68 k_B T$, and $W = 0.35 k_B T$ as narrow resonances in (b), (e), and (f), respectively

operators for scattering states in the open channels, and V is the volume of the system. $\hat{b}^\dagger$ and $\hat{b}$ are the creation and annihilation operators of the two-body bound state in the closed channel, and ν is the detuning of the molecular state in the closed channel. The last term denotes the conversion between the open-channel scattering states and the closed-channel molecular state, with the strength given by α. The ladder diagram for the two-channel model is shown in Fig. 6. The summation of the ladder diagram leads to the Schwinger-Dyson equation,

$$T_2(E) = g + \frac{|\alpha|^2}{E - \nu} + \left(g + \frac{|\alpha|^2}{E - \nu}\right)\frac{1}{V}\sum_{\mathbf{k}}\frac{1}{E - \mathbf{k}^2/m}T_2(E),$$
(B2)

which leads to

$$T_2(E) = \frac{g + \frac{|\alpha|^2}{E - \nu}}{1 - \left(g + \frac{|\alpha|^2}{E - \nu}\right)\frac{1}{V}\sum_{\mathbf{k}}\frac{1}{E - \mathbf{k}^2/m}}.$$
(B3)

Notice that the T matrix given in Eq. (B3) is renormalizable. This two-body T matrix should be related to the s-wave scattering amplitude, and therefore we have

$$T_2(E = 0) = -\frac{4\pi}{m}f_0(k = 0) = \frac{4\pi}{m}a_{\text{bg}}\left(1 - \frac{\Delta}{B - B_{\text{res}}}\right).$$
(B4)

It should be noticed that by equaling T_2 in Eq. (B4) and that give by the zero-range model in Eq. (B3), we can build the relations between the bare parameters in Eq. (B1). In addition, features of Feshbach resonance can also be encapsulated by the zero-range model, including the s_{res} parameter.

We also define $\nu = \delta\mu_B(B - B_{\text{res}}) + \nu_p$. When detuning the magnetic field away from the resonance position $|B - B_{\text{res}}| \gg |\Delta|$, we have

$$T_2(E = 0) = \frac{4\pi}{m}a_{\text{bg}} = \frac{1}{\frac{1}{g} + \frac{1}{V}\sum_{\mathbf{k}}\frac{1}{\mathbf{k}^2/m}}.$$
(B5)

Hence, we reach the renormalization identity that relates g to a physical quantity a_{bg},

$$\frac{1}{g} = \frac{m}{4\pi a_{\text{bg}}} - \Lambda,$$
(B6)

where Λ denotes

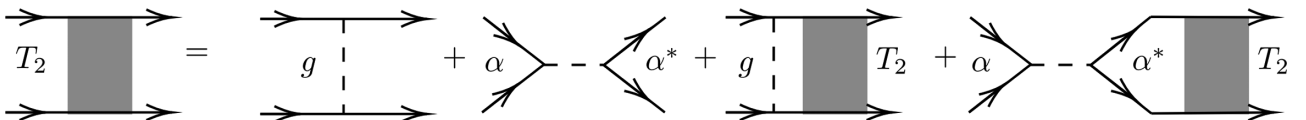$$\Lambda = \frac{1}{V}\sum_{\mathbf{k}}\frac{1}{\mathbf{k}^2/m}.$$
(B7)

FIG. 6. Ladder diagrams for two-body scattering T matrix of the two-channel model.

By comparing Eq. (B3) with Eq. (B4) and using the relation between g and a_{bg}, the remainder renormalization conditions can be given by

$$\frac{1}{\alpha} = \left(1 - \frac{4\pi a_{\text{bg}}}{m}\Lambda\right)\sqrt{\frac{m}{4\pi a_{\text{bg}}\delta\mu_B\Delta}}, \qquad \text{(B8)}$$

$$\nu = \delta\mu_B(B - B_{\text{res}}) + \frac{\Lambda}{1 - \frac{4\pi a_{\text{bg}}}{m}\Lambda}\frac{4\pi a_{\text{bg}}\delta\mu_B\Delta}{m}. \qquad \text{(B9)}$$

By substituting Eqs. (B6), (B8), and (B9) into Eq. (B3), we have

$$T_2 = \frac{4\pi/m}{\frac{E - \delta\mu_B(B - B_{\text{res}})}{a_{\text{bg}}[E + \delta\mu_B\Delta - \delta\mu_B(B - B_{\text{res}})]} - \sqrt{-mE}}. \qquad \text{(B10)}$$

[1] C. Chin, R. Grimm, P. Julienne, and E. Tiesinga, Feshbach resonances in ultracold gases, Rev. Mod. Phys. **82**, 1225 (2010).

[2] T. Köhler, K. Góral, and P. S. Julienne, Production of cold molecules via magnetically tunable feshbach resonances, Rev. Mod. Phys. **78**, 1311 (2006).

[3] P. Makotyn, C. E. Klauss, D. L. Goldberger, E. A. Cornell, and D. S. Jin, Universal dynamics of a degenerate unitary Bose gas, Nat. Phys. **10**, 116 (2014).

[4] C. Eigen, J. A. P. Glidden, R. Lopes, N. Navon, Z. Hadzibabic, and R. P. Smith, Universal Scaling Laws in the Dynamics of a Homogeneous Unitary Bose Gas, Phys. Rev. Lett. **119**, 250404 (2017).

[5] M. Prüfer, P. Kunkel, H. Strobel, S. Lannig, D. Linnemann, C.-M. Schmied, J. Berges, T. Gasenzer, and M. K. Oberthaler, Observation of universal dynamics in a spinor Bose gas far from equilibrium, Nature (London) **563**, 217 (2018).

[6] S. Erne, R. Bücker, T. Gasenzer, J. Berges, and J. Schmiedmayer, Universal dynamics in an isolated one-dimensional Bose gas far from equilibrium, Nature (London) **563**, 225 (2018).

[7] C. Eigen, J. A. P. Gliden, R. Lopes, E. A. Cornel, R. P. Smith, and Z. Hadzibabic, Universal prethermal dynamics of Bose gases quenched to unitarity, Nature (London) **563**, 221 (2018).

[8] R. Saint-Jalm, P. C. M. Castilho, E. Le Cerf, B. Bakkali-Hassani, J.-L. Ville, S. Nascimbene, J. Beugnon, and J. Dalibard, Dynamical Symmetry and Breathers in a Two-Dimensional Bose Gas, Phys. Rev. X **9**, 021035 (2019).

[9] S. Deng, Z.-Y. Shi, P. Diao, Q. Yu, H. Zhai, R. Qi, and H. Wu, Observation of the Efimovian expansion in scale-invariant Fermi gases, Science **353**, 371 (2016).

[10] J. Hu, L. Feng, Z. Zhang, and C. Chin, Quantum simulation of Unruh radiation, Nat. Phys. **15**, 785 (2019).

[11] C. Lv, R. Zhang, and Q. Zhou, $SU(1, 1)$ Echoes for Breathers in Quantum Gases, Phys. Rev. Lett. **125**, 253002 (2020).

[12] Y.-Y. Chen, P. Zhang, W. Zheng, Z. Wu, and H. Zhai, Many-body echo, Phys. Rev. A **102**, 011301(R) (2020).

[13] D. A. Abanin, E. Altman, I. Bloch, and M. Serbyn, Colloquium: Many-body localization, thermalization, and entanglement, Rev. Mod. Phys. **91**, 021001 (2019).

[14] C. Wang, P. Zhang, X. Chen, J. Yu, and H. Zhai, Scheme to Measure the Topological Number of a Chern Insulator from Quench Dynamics, Phys. Rev. Lett. **118**, 185701 (2017).

[15] M. Tarnowski, F. N. Ünal, N. Fläschner, B. S. Rem, A. Eckardt, K. Sengstock, and C. Weitenberg, Measuring topology from dynamics by obtaining the Chern number from a linking number, Nat. Commun. **10**, 1728 (2019).

[16] W. Sun, C.-R. Yi, B.-Z. Wang, W.-W. Zhang, B. C. Sanders, X.-T. Xu, Z.-Y. Wang, J. Schmiedmayer, Y. Deng, X.-J. Liu, S.

Chen, and J.-W. Pan, Uncover Topology by Quantum Quench Dynamics, Phys. Rev. Lett. **121**, 250403 (2018).

[17] C. Gao, H. Zhai, and Z.-Y. Shi, Dynamical Fractal in Quantum Gases with Discrete Scaling Symmetry, Phys. Rev. Lett. **122**, 230402 (2019).

[18] C. Gao, M. Sun, P. Zhang, and H. Zhai, Universal Dynamics of a Degenerate Bose Gas Quenched to Unitarity, Phys. Rev. Lett. **124**, 040403 (2020).

[19] M. Sun, P. Zhang, and H. Zhai, High Temperature Virial Expansion to Universal Quench Dynamics, Phys. Rev. Lett. **125**, 110404 (2020).

[20] D. J. M. Ahmed-Braun, S. Musolino, V. E. Colussi, and S. J. J. M. F. Kokkelmans, Evolution of the unitary Bose gas for broad to narrow Feshbach resonances, Phys. Rev. A **106**, 013315 (2022).

[21] V. E. Colussi, B. E. van Zwol, J. P. D'Incao, and S. J. J. M. F. Kokkelmans, Bunching, clustering, and the buildup of few-body correlations in a quenched unitary Bose gas, Phys. Rev. A **99**, 043604 (2019).

[22] S. Musolino, H. Kurkjian, M. Van Regemortel, M. Wouters, S. J. J. M. F. Kokkelmans, and V. E. Colussi, Bose-Einstein Condensation of Efimovian Triples in the Unitary Bose Gas, Phys. Rev. Lett. **128**, 020401 (2022).

[23] G. Rupak, Universality in a 2-Component Fermi System at Finite Temperature, Phys. Rev. Lett. **98**, 090403 (2007).

[24] X.-J. Liu, H. Hu, and P. D. Drummond, Virial Expansion for a Strongly Correlated Fermi Gas, Phys. Rev. Lett. **102**, 160401 (2009).

[25] X.-J. Liu, H. Hu, and P. D. Drummond, Three attractively interacting fermions in a harmonic trap: Exact solution, ferromagnetism, and high-temperature thermodynamics, Phys. Rev. A **82**, 023619 (2010).

[26] X.-J. Liu, Virial expansion for a strongly correlated Fermi system and its application to ultracold atomic Fermi gases, Phys. Rep. **524**, 37 (2013).

[27] S.-G. Peng, S.-Q. Li, P. D. Drummond, and X.-J. Liu, High-temperature thermodynamics of strongly interacting s-wave and p-wave Fermi gases in a harmonic trap, Phys. Rev. A **83**, 063618 (2011).

[28] S.-G. Peng, S.-H. Zhao, and K. Jiang, Virial expansion of a harmonically trapped Fermi gas across a narrow Feshbach resonance, Phys. Rev. A **89**, 013603 (2014).

[29] Y. Yan and D. Blume, Energy and structural properties of n-boson clusters attached to three-body Efimov states: Two-body zero-range interactions and the role of the three-body regulator, Phys. Rev. A **92**, 033626 (2015).

[30] Y. Yan and D. Blume, Path-Integral Monte Carlo Determination of the Fourth-Order Virial Coefficient for a Unitary

Two-Component Fermi Gas with Zero-Range Interactions, Phys. Rev. Lett. **116**, 230401 (2016).

[31] M. Sun and X. Cui, Enhancing the Efimov correlation in Bose polarons with large mass imbalance, Phys. Rev. A **96**, 022707 (2017).

[32] Y. Nishida, Viscosity spectral functions of resonating fermions in the quantum virial expansion, Ann. Phys. **410**, 167949 (2019).

[33] Y. Hou and J. E. Drut, Virial expansion of attractively interacting Fermi gases in one, two, and three dimensions, up to fifth order, Phys. Rev. A **102**, 033319 (2020).

[34] Y. Hou, K. J. Morrell, A. J. Czejdo, and J. E. Drut, Fourth- and fifth-order virial expansion of harmonically trapped fermions at unitarity, Phys. Rev. Res. **3**, 033099 (2021).

[35] M. Sun, H. Zhai, and X. Cui, Visualizing the Efimov Correlation in Bose Polarons, Phys. Rev. Lett. **119**, 013401 (2017).

[36] D. B. Kaplan and S. Sun, New Field-Theoretic Method for the Virial Expansion, Phys. Rev. Lett. **107**, 030601 (2011).

[37] T. Bourdel, J. Cubizolles, L. Khaykovich, K. M. F. Magalhães, S. J. J. M. F. Kokkelmans, G. V. Shlyapnikov, and C. Salomon, Measurement of the Interaction Energy near a Feshbach Resonance in a ^{6}Li Fermi Gas, Phys. Rev. Lett. **91**, 020402 (2003).

[38] J. T. Stewart, J. P. Gaebler, and D. S. Jin, Using photoemission spectroscopy to probe a strongly interacting Fermi gas, Nature (London) **454**, 744 (2008).

[39] S. Nascimbène, N. Navon, K. J. Jiang, F. Chevy, and C. Salomon, Exploring the thermodynamics of a universal Fermi gas, Nature (London) **463**, 1057 (2010).

[40] E. D. Kuhnle, S. Hoinka, P. Dyke, H. Hu, P. Hannaford, and C. J. Vale, Temperature Dependence of the Universal Contact Parameter in a Unitary Fermi Gas, Phys. Rev. Lett. **106**, 170402 (2011).

[41] M. Feld, B. Fröhlich, E. Vogt, M. Koschorreck, and M. Köhl, Observation of a pairing pseudogap in a two-dimensional Fermi gas, Nature (London) **480**, 75 (2011).

[42] M. J. H. Ku, A. T. Sommer, L. W. Cheuk, and M. W. Zwierlein, Revealing the superfluid lambda transition in the universal thermodynamics of a unitary Fermi gas, Science **335**, 563 (2012).

[43] B. Mukherjee, P. B. Patel, Z. Yan, R. J. Fletcher, J. Struck, and M. W. Zwierlein, Spectral Response and Contact of the Unitary Fermi Gas, Phys. Rev. Lett. **122**, 203402 (2019).

[44] C. Carcy, S. Hoinka, M. G. Lingham, P. Dyke, C. C. N. Kuhn, H. Hu, and C. J. Vale, Contact and Sum Rules in a Near-Uniform Fermi Gas at Unitarity, Phys. Rev. Lett. **122**, 203401 (2019).

[45] T.-L. Ho and E. J. Mueller, High Temperature Expansion Applied to Fermions near Feshbach Resonance, Phys. Rev. Lett. **92**, 160404 (2004).

[46] Z. Yu, J. H. Thywissen, and S. Zhang, Universal Relations for a Fermi Gas Close to a p-Wave Interaction Resonance, Phys. Rev. Lett. **115**, 135304 (2015).

[47] E. Marcelino, A. Nicolai, I. Roditi, and A. LeClair, Virial coefficients for trapped Bose and Fermi gases beyond the unitary limit: An s-matrix approach, Phys. Rev. A **90**, 053619 (2014).

[48] T.-L. Ho, X. Cui, and W. Li, Alternative Route to Strong Interaction: Narrow Feshbach Resonance, Phys. Rev. Lett. **108**, 250401 (2012).

[49] S.-G. Peng, X.-J. Liu, H. Hu, and S.-Q. Li, Non-universal thermodynamics of a strongly interacting inhomogeneous Fermi gas using the quantum virial expansion, Phys. Lett. A **375**, 2979 (2011).

[50] H. Tajima, S. Tsutsui, T. M. Doi, and K. Iida, Unitary p-wave Fermi gas in one dimension, Phys. Rev. A **104**, 023319 (2021).

[51] J. Hofmann, High-temperature expansion of the viscosity in interacting quantum gases, Phys. Rev. A **101**, 013620 (2020).

[52] M. He, S. Zhang, H. M. Chan, and Q. Zhou, Concept of a Contact Spectrum and Its Applications in Atomic Quantum Hall States, Phys. Rev. Lett. **116**, 045301 (2016).

[53] M. He, C. Lv, H.-Q. Lin, and Q. Zhou, Universal relations for ultracold reactive molecules, Sci. Adv. **6**, eabd4699 (2020).

[54] B. Gao, Quantum-defect theory of atomic collisions and molecular vibration spectra, Phys. Rev. A **58**, 4222 (1998).

[55] B. Gao, E. Tiesinga, C. J. Williams, and P. S. Julienne, Multichannel quantum-defect theory for slow atomic collisions, Phys. Rev. A **72**, 042719 (2005).

[56] H. Zhai, *Ultracold Atomic Physics* (Cambridge University Press, Cambridge, England, 2021).

[57] V. E. Colussi, H. Kurkjian, M. Van Regemortel, S. Musolino, J. van de Kraats, M. Wouters, and S. J. J. M. F. Kokkelmans, Cumulant theory of the unitary Bose gas: Prethermal and Efimovian dynamics, Phys. Rev. A **102**, 063314 (2020).

[58] V. E. Colussi, J. P. Corson, and J. P. D'Incao, Dynamics of Three-Body Correlations in Quenched Unitary Bose Gases, Phys. Rev. Lett. **120**, 100401 (2018).

[59] J. P. D'Incao, J. Wang, and V. E. Colussi, Efimov Physics in Quenched Unitary Bose Gases, Phys. Rev. Lett. **121**, 023401 (2018).